RSC Advances

PAPER

View Article Online
View Journal | View Issue

Cite this: *RSC Adv.*, 2018, **8**, 4273

Hydrothermal synthesis of montmorillonite/hydrochar nanocomposites and application for 17β-estradiol and 17α-ethynylestradiol removal

Si-rong Tian,[ab] Yun-guo Liu,[*ab] Shao-bo Liu,[cd] Guang-ming Zeng,[ab] Lu-hua Jiang,[ab] Xiao-fei Tan,[ab] Xi-xian Huang,[ab] Zhi-hong Yin,[ab] Ni Liu[ab] and Jiang Li[ab]

With a view to reducing estrogens pollution in aqueous environments, montmorillonite/hydrochar (MMT/HC) with or without modification by KOH *via* hydrothermal carbonization process (HTC) were applied to remove 17β-estradiol (E2) and 17α-ethynylestradiol (EE2). The characterizations of MMT/HC indicated that MMT had been successfully attached onto HC surface, which could cause an improvement in the stability of the clay nanoparticles. MMT/HC with 1% KOH (MMT/HC-K1) exhibited excellent adsorption ability (E2: Q_m = 138 mg g^{-1}, EE2: Q_m = 69 mg g^{-1}) compared to those of other adsorbents; approximately 2-fold higher than that of HC. Moreover, the adsorption capacity maintained a high level over a wide pH range (2–8). The pseudo-second-order model and Freundlich model exhibited prior fitting performance for adsorption of E2 and EE2. The regenerated MMT/HC-K1 retained over 80% of its initial capacity after four cycles. The adsorption mechanism on MMT/HC-K1 could be explained by hydrophobicity, π–π bond, electrostatic interaction and H-bonding interaction. Overall, MMT/HC-K1 synthesis from two low-cost materials, could be considered as a competitive adsorbent for estrogens removal from aqueous environment, considering its high adsorption capacity and regeneration ability.

Received 3rd November 2017
Accepted 7th January 2018

DOI: 10.1039/c7ra12038a

rsc.li/rsc-advances

1. Introduction

Endocrine-disrupting chemicals (EDCs), widely existing in water in the environment as well as in drinking water,[1] have gained growing concern in recent years. EDCs are classified into natural and synthetic estrogens, such as 17β-estradiol (E2) and 17α-ethynylestradiol (EE2), respectively.[2] These compounds are composed a group of emerging microcontaminants that cause adverse health effects, including endocrine malfunction, and developmental and reproductive disorders.[3–5] There are direct or indirect effects on the normal hormone activities *via* receptor-mediated processes mimicking endogenous hormones.[2] Some studies also show that estrogens have potential risks to fish and other aquatic organisms at low concentration of ng L^{-1} levels.[2,6,7] Thus, it is necessary to remove estrogens in aqueous environments.

Several technologies have been used to remove estrogens from water such as biological treatment and advanced oxidation processes (AOPs).[8] However, some problematic shortcomings of these technologies cannot be overlooked, which would limit their further application. For instance, AOPs demand high energy, and generate hazardous by-products simultaneously.[8,9] Thus, further studies are essential to explore efficient technologies. Recently, adsorption has been considered as an efficient, available and recyclable technique for the removal of estrogen from water.[10–12] Sun and Zhou had reported that multi-walled carbon nanotubes (MWCNTs) was used as an adsorbent to remove E2.[13] The industrialgrade polyamide 612 (PA612) particles rapidly removed EE2 and showed a selective adsorption process.[14] Jarosova *et al.*[15] observed that the most plausible removal mechanisms of E2 and EE2 by nanoscale zero-valent iron (nZVI) particles were sorption and nonspecific oxygen-mediated oxidation of estrogens. Magnetic reduced graphene oxides for removal of 4-*n*-nonylphenol (4-*n*-NP) and bisphenol A (BPA) exhibited excellent adsorption performance and simple magnetic separation.[16] Moreover, the application of composite materials in adsorbing pollutants has attracted increasing public concern due to their superior properties such as higher removal efficiency and easier modified properties.[17,18] Banerjee *et al.*[19] produced Metal Organic Framework (MOF)-carbon-Fe_3O_4 nanoparticles with high surface area and porous structures that as a superadsorbent for removal of environmental pollutants,

[a]*College of Environmental Science and Engineering, Hunan University, Changsha 410082, P. R. China. E-mail: hnuliuyunguo@gmail.com; liuyunguo@hnu.edu.cn; Fax: +86 731 88822829; Tel: +86 731 88649208*

[b]*Key Laboratory of Environmental Biology and Pollution Control, Hunan University, Ministry of Education, Changsha 410082, P. R. China*

[c]*School of Metallurgy and Environment, Central South University, Changsha 410083, P. R. China*

[d]*College of Environmental Science and Engineering Research, Central South University of Forestry and Technology, Changsha 410004, P. R. China*

like oil/hydrocarbon, dye and phenol. But synthesis of char on biomass and clay nanocomposites for the removal of estrogens has not yet been reported.

Montmorillonite (MMT), a clay mineral that widely used in medical-treatment and environmental pollution treatment, has been proven to display high adsorptive affinities for cationic chemicals.[20] Moreover, MMT has been studied for the removal of organic materials from water and soil,[21,22] considering its unique properties such as large surface areas, lamellar structure, low cost and high degree of swelling.[17,23] In particular, its layers are negatively charged that is normally balanced by hydrated cations placed in the interlayer spaces.[24] Açışlı *et al.*[23] applied MMT to adsorb surfactants, and found that the adsorbed amount of surfactants were highly related to the hydrophobic interactions. Nevertheless, MMT is a kind of ultrafine particles (*i.e.*, colloids/nanoparticles), and is unsuitable for large-scale applications in water treatment facilities as fixed-bed media or flocculation additives.[25]

In order to extend the environmental application of MMT, the synthesis of novel char-based composites material loaded of MMT could be a good choice. Hydrochar (HC) has been used to remove the organic pollutants from aqueous solutions as it is harmless and porous material with large specific surface area.[26,27] Liu and Zhang[28] reported that HC possessed irregular surface and much oxygen-containing groups. Moreover, HC serves as a good porous structure to support and host the distribution of the nanoparticles within its matrix. Considering these characterizations, the method that combination of MMT and HC were cost-efficient and facile, as well as suitable for large-scale productions.[27]

In this study, montmorillonite/hydrochar nanocomposites (MMT/HC) with modification by KOH were applied to uptake of E2 and EE2. The physicochemical properties of these adsorbents were characterized. The kinetics and isotherms of adsorption on the samples have been analyzed. In addition, the sustainable utilization was evaluated by adsorption cycles. In the end, the relevant mechanisms for estrogens removal were identified.

2. Experimental section

2.1 Materials

The 17β-estradiol (E2, $C_{18}H_{24}O_2$, 98%, USA) and 17α-ethinylestradiol (EE2, $C_{18}H_{22}O_2$, 98%, UAS) were supplied from Sigma-Aldrich Corp, and their physicochemical properties and structures are shown in Table 1. Montmorillonite was purchased from Aladdin Industrial Corporation and rice husk biomass obtained from the farm in Yiyang, Hunan province, China. The ultrapure water (18.25 M Ω) was produced by Millipore Milli-Q water purification system. Other chemicals were analytical reagent grade and provided by Shanghai Chemical Corp.

2.2 Synthesis of MMT/HCs

MMT/HCs were prepared by MMT and HC nanocomposites *via* hydrothermal carbonization process (HTC). Specifically, MMT was dissolved in 70 mL of rice husk biomass dispersion with the MMT and biomass ratio of 1 : 1 (2.5 g : 2.5 g). The mixed solution was heated at 180 °C in an autoclave (100 mL in capacity) and maintained for 16 h at this temperature, and then cooled down to room temperature. The obtained carbonaceous mixture was thoroughly flushed with deionized water, immersed in methanol, and finally dried at 90 °C for 24 h. The collected material was denoted as MMT/HC.

The MMT/HC was further chemically modified by KOH. To ensure successful modification, the material was ground and the reaction of KOH solution was keep for 4 h. The products were dried at 90 °C for 14 h. Finally, the products were squashed and stored in sealing bag in the desiccators. Three mass ratios were employed (KOH: MMT/HC = 1%, 4% and 8%) and they were named as MMT/HC-K1, MMT/HC-K4 and MMT/HC-K8, respectively.

2.3 Characterization

The thermogravimetric analysis (TGA) was conducted by using a TGAQ 5000 instrument under a high-purity helium gas flow. The X-ray diffraction (XRD) was measured by a Rigaku D/max-C X-ray diffractometer (at 40 kV and 20 mA) with Cu Kα radiation to confirm the crystal phases of the MMT/HCs. The surface chemical properties of MMT/HCs were confirmed by Fourier transform infrared (FTIR) spectrophotometer, recorded in the range from 4000 to 400 cm^{-1} at room temperature (Nicolet 6700 spectrometer, USA). The elemental composition of MMT/HCs was measured by an elemental analyzer (Vario EL III, Elementar, Germany). The Brunauer–Emmett–Teller surface area (BET) and porosities of the MMT/HCs were carried out by Quantachrome Instruments Quadrasorb SI. The structures and surface morphologies of MMT/HCs were observed by scanning electron microscopy (SEM, Nova Nanosem 230, USA) and transmission electron microscopy (TEM, JEM-3010, Japan).

2.4 Adsorption experiments

The stock solutions (2.5 mg mL^{-1}) of estrogen were prepared by dissolution of E2 and EE2 powder in methanol and then diluted successively with ultrapure water to obtain desired concentrations in the following experiments. In this study, a precise amount of MMT/HCs (5 mg) was put into E2 or EE2 solution (100 mL) with a fixed concentration. Adsorbent and adsorbates were mixed well in conical flask for 24 h at 25 °C using a thermostatic shaker bath with 170 rpm. Shaking for a scheduled time, the solution was centrifuged and filtered by a syringe filter (polytetrafluoroethylene, 0.45 μm). To explore the adsorption estrogen capacity under various pH conditions, the pH values of solutions were adjusted by 0.1 M HCl and NaOH solution to a desired value. The adsorption isotherms for estrogen over MMT/HCs were obtained by adsorption for 24 h using various initial concentrations of estrogen solutions; kinetics experiments were conducted by different time intervals. Regeneration measurements were conducted by the ethanol desorption technique. The adsorbed MMT/HCs were centrifuged for 5 min, washed with 20 mL ethanol and deionized water for several times, and then, dried at 90 °C. The regenerated MMT/HCs were applied to the next estrogen adsorption cycle. The regeneration

Table 1 Physicochemical properties and structure of E2 and EE2

Estrogen	Mol. wt[a] (g mol^{-1})	S_w[a] (mg L^{-1} at 20 °C)	log K_{ow}[a]	pK_a[b]	Structure
17β-estradiol, E2	272.4	13	3.94	10.4	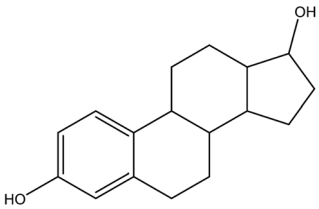
17α-ethynylestradiol, EE2	296.4	4.8	4.15	10.5	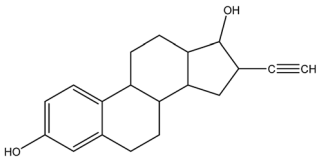

[a] Ref. 58. [b] Ref. 59.

experiment was followed four cycles. The adsorption estrogen capacity was calculated by the reported methods.[22,29] The concentrations of estrogen were measured by F-4500 fluorescence spectrophotometer (Hitachi, Japan). The parameters were set as described in previous studies.[6,30]

3. Results and discussion

3.1 Characterization of MMT/HCs

3.1.1 XRD. XRD has been applied to study the microstructure of clay mineral.[31] Fig. 1 displays the XRD patterns of MMT/HCs samples. As can be seen, MMT sample exhibited the main diffraction peaks, which was agreed with the characteristic smectite peak.[20,32] After attached to HC and KOH, it can be seen that the similar typical diffraction peaks to those of MMT, suggesting the remained of the layered structural characteristics of MMT. However, the major reflection on MMT at 6.18° was shifted the diffraction angles after hydrothermal synthesis. The intensity of this peak decreased, indicated the original clay layer structures to be disrupted to some extent.[20] The characteristic peak of MMT/HCs at 26.70° sample was obviously centered corresponded to the reflection of rice husk char,[33] suggesting a low degree of crystallinity on synthesizing MMT/HCs.

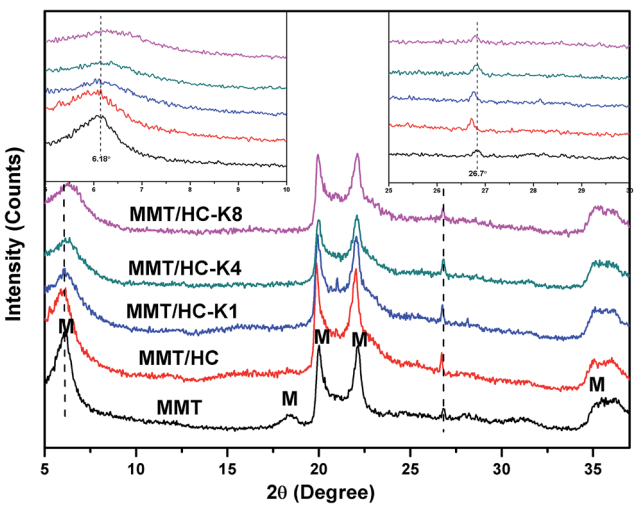

Fig. 1 XRD patterns of the adsorbents (M: montmorillonite).

3.1.2 SEM and TEM. Scanning electron microscopy (SEM) and transmission electron microscope (TEM) were carried out to observe surface morphologies and shapes of adsorbents. As shown in Fig. 2 and 3, it can be seen that MMT displayed large particle form, flat shape, layer structure and a smooth surface, which was well consistent with previous study.[34] Meanwhile, there were some apparent differences in the morphology of the mineral surfaces after MMT combined with rice husk biomass *via* HTC process. SEM images clearly show some MMT particles adhered on MMT/HCs surfaces which were not found on HC surfaces. HC was used as a media for supporting MMT which could cause the improvement of clay particles stability. The raising carbon content in results of element analysis verified that MMT was successfully combined with HC (Table 2).

3.1.3 BET. The measured BET surface area of HC, MMT and MMT/HCs nanocomposites are summarized in Table 2. Compared to the BET surface area of HC (8 m^2 g^{-1}) and MMT (20 m^2 g^{-1}), MMT/HC developed to 40 m^2 g^{-1}, which were caused by the formation of nanoparticles to extend the surface area. The BET surface area of MMT/HC-Ks declined slightly when MMT/HC was graft by KOH but still higher than that of raw HC and MMT, since new crystals in plate-like, fibrous, granular forms might block pores on the surface of MMT/HC-Ks, and the formation of crystals was enhanced by increasing of KOH concentration.[35] The nitrogen adsorption–desorption isotherms and pore size distribution of all samples are show in Fig. 4 and 5, respectively. According to the traditional classification of Brunauer, Deming, Deming and Teller (BDDT), adsorption isotherms of HC resembled those of type IV and Langmuir adsorption isotherms (type I) in the region of low relative pressure, which suggested that HC had micro- and

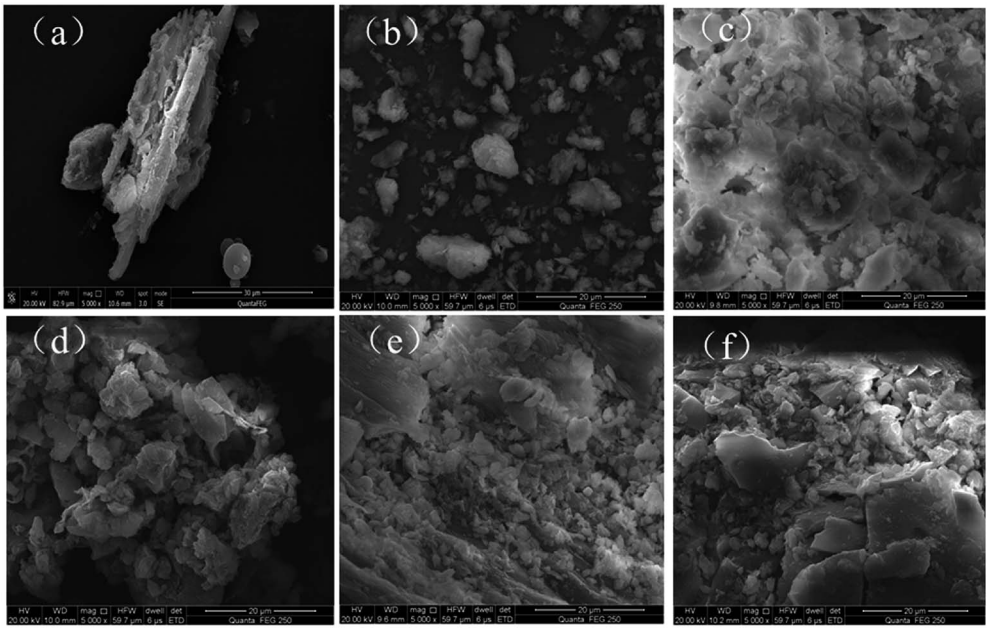

Fig. 2 SEM images of (a) HC, (b) MMT, (c) MMT/HC, (d) MMT/HC-K1, (e) MMT/HC-K4 and (f) MMT/HC-K8.

mesoporous structures. The adsorption isotherms of MMT and MMT/HCs were assigned to type IV, corresponding to mesoporous structure.[36] Moreover, the hysteresis loops belonged to a type H3 in the classification of IUPAC,[37] indicating the representative of slit-shaped pores. It could exist finer intra-aggregated pores in intra-agglomerated primary particles at lower relative pressure range ($P/P_0 < 0.46$), and the larger inter-aggregated pores in inter-aggregated secondary particles at higher relative pressure range ($0.6 < P/P_0 < 0.9$).[20] Additional, the distribution of pore sizes were calculated Barrett–Joyner–Halenda (BJH) (Fig. 5). The average pore diameter was estimated to be 3.6–3.9 nm for all samples and HC present a special peak at 1.76 nm, which meant that the adsorbents were dominated by meso-size level and HC at micro/meso-size levels.

3.1.4 FTIR. FTIR spectroscopy was utilized to investigate the functional groups of these adsorbents (Fig. 6a). Characteristic peaks at 3623 cm^{-1} and 3436 cm^{-1} were corresponded to O–H stretching[20] and hydrogen bonded water molecule,[38]

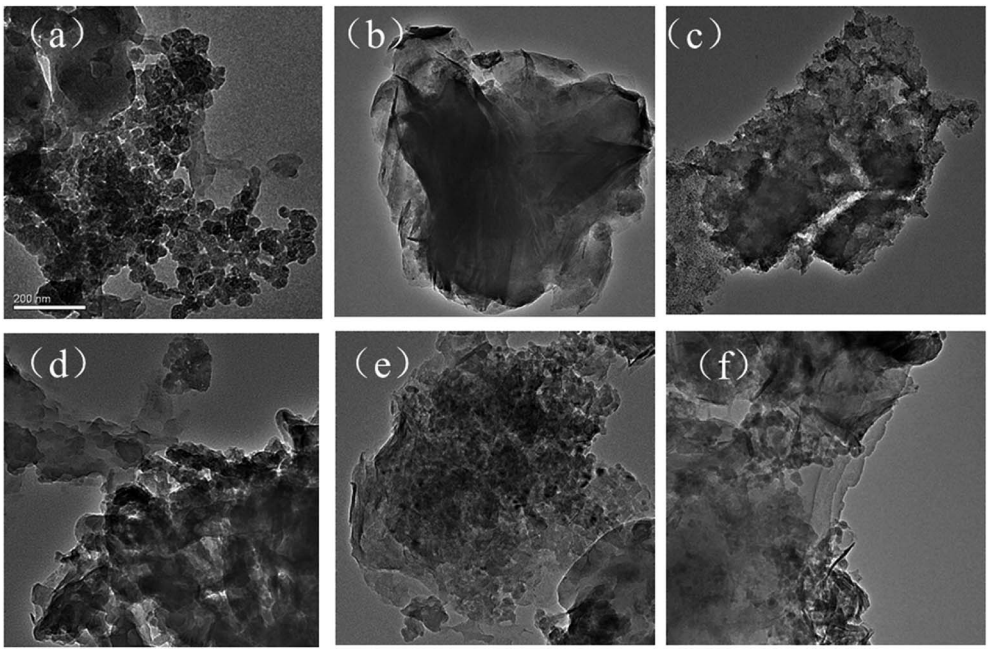

Fig. 3 TEM images of (a) HC, (b) MMT, (c) MMT/HC, (d) MMT/HC-K1, (e) MMT/HC-K4 and (f) MMT/HC-K8.

Table 2 The BET data and elemental composition of the adsorbents

	BET surface area ($m^2\ g^{-1}$)	Pore volume ($cm^3\ g^{-1}$)	C (%)	H (%)	C/H
HC	8	0.041	45.01	4.917	0.109
MMT	20	0.126	0.292	2.33	0.125
MMT/HC	49	0.118	18.95	2.79	6.79
MMT/HC-K1	37	0.106	18.79	2.58	7.28
MMT/HC-K4	39	0.115	19.19	2.79	6.88
MMT/HC-K8	36	0.085	17.25	2.67	6.46

respectively. The peaks at 1620 cm^{-1} were attributed to the band of C=C.[34] Clearly, the spectra in the region of 1050–450 cm^{-1} were split into three components at approximately 1041, 522 and 466 cm^{-1}, which were corresponded to Si–O–Si groups of tetrahedral sheet, the deformation modes of the Si–O bond and the bending modes of the Si–O bond, respectively.[39] Compared to MMT and HC, MMT/HC generated a new bond of carbonyl groups (C–O–H) at peak of 1388 cm^{-1},[40] it represented of the chemical interaction between MMT and HC in the composites. After treated by KOH, weaker Si–O bond were showed in the FTIR spectrum of MMT/HCs. Moreover, the density of OH functions increased.

3.1.5 TGA. The thermogravimetric analysis (TGA) curves of these adsorbents are shown in Fig. 6b, which show the differential mass loss as the variation of temperature. When the temperature was below 100 °C, the major mass loss might be attributed to the removal of free water molecules. In this stage, the mass loss content increased progressively with KOH content increased 4%. The curves showed a steady weight at 100–250 °C, and MMT was the most unstable of these samples at this stage. At the temperature range of 300–500 °C, the mass loss should be attributed to the decomposition of the cellulose and hemicellulose of rice husk biochar.[41–43] At the temperature higher than 600 °C, the samples achieved a state of balance, and the mass residual of modified materials were less than MMT (82.98%), revealed that the thermal stability of MMT/HCs was weakened, which was in uniformity with the previous study.[36,38] However, joined KOH, the thermal stability of MMT/HC-Ks were advanced (1–6%) than that of MMT/HC. This slight advance may be due to the chemical bonding in the system of organic–inorganic composite.[44]

3.2 Adsorptive removal of estrogen using MMT/HCs

3.2.1 Adsorption kinetics. Adsorption kinetics is a dominant channel to investigate the adsorption mechanism and potential rate-controlling steps.[45] The pseudo-first-order kinetic model and pseudo-second-order kinetic model were used to analyze adsorption kinetics data and the models were given as eqn (1) and eqn (2), respectively:

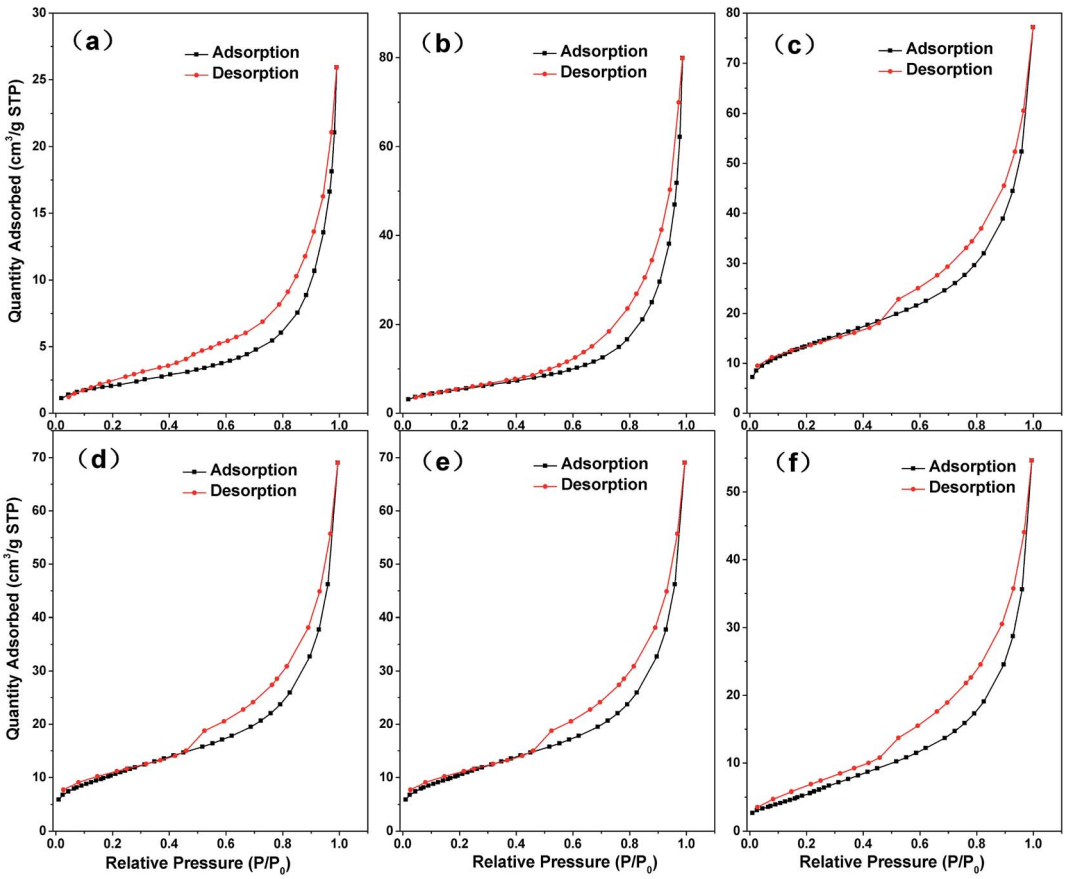

Fig. 4 N_2 adsorption–desorption curve of (a) HC, (b) MMT, (c) MMT/HC, (d) MMT/HC-K1, (e) MMT/HC-K4 and (f) MMT/HC-K8.

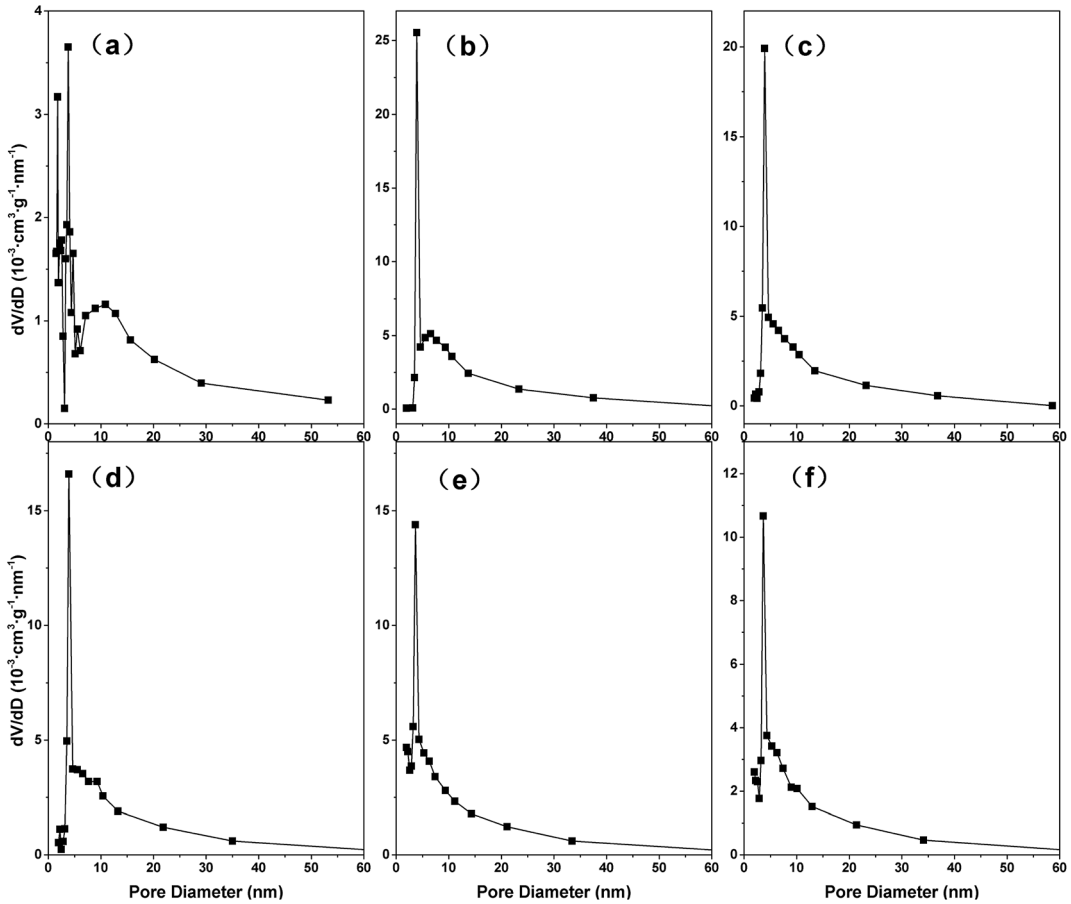

Fig. 5 Pore size distribution of (a) HC, (b) MMT, (c) MMT/HC, (d) MMT/HC-K1, (e) MMT/HC-K4 and (f) MMT/HC-K8.

$$\ln(Q_e - Q_t) = \ln Q_e - k_1 t \quad (1)$$

$$\frac{t}{Q_t} = \frac{1}{k_2 Q_e^2} + \frac{t}{Q_e} \quad (2)$$

where Q_e and Q_t (mg g^{-1}) are the adsorbed amount of E2 or EE2 at equilibrium and time t (h), respectively. k_1 (1/h) and k_2 (g mg^{-1} h^{-1}) are the adsorption rate constant of pseudo-first-order and pseudo-second-order, respectively.[46]

Fig. 7 shows the kinetics for the adsorption of E2 and EE2 by HC and MMT/HCs. It is clear that the adsorption of estrogens reached equilibrium after 6 h and 4 h, respectively. From kinetics images, MMT/HC-K1 exhibited excellent adsorption ability than other adsorbents, and it approximately 2-fold higher than that of HC. The simulated parameters of two kinetics models are listed in Table 3. Obviously, the pseudo-second-order kinetic model showed excellent adaptability to the experimental data, since the R^2 values were closer to 1 than

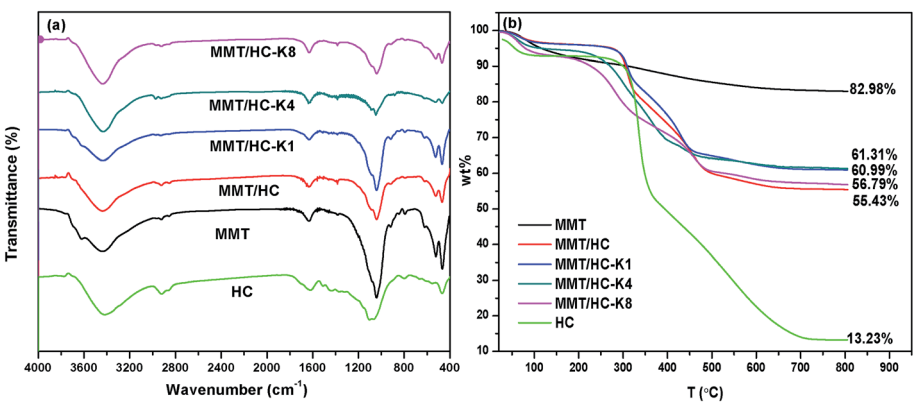

Fig. 6 (a) FTIR spectra and (b) TGA curves of MMT and MMT/HCs.

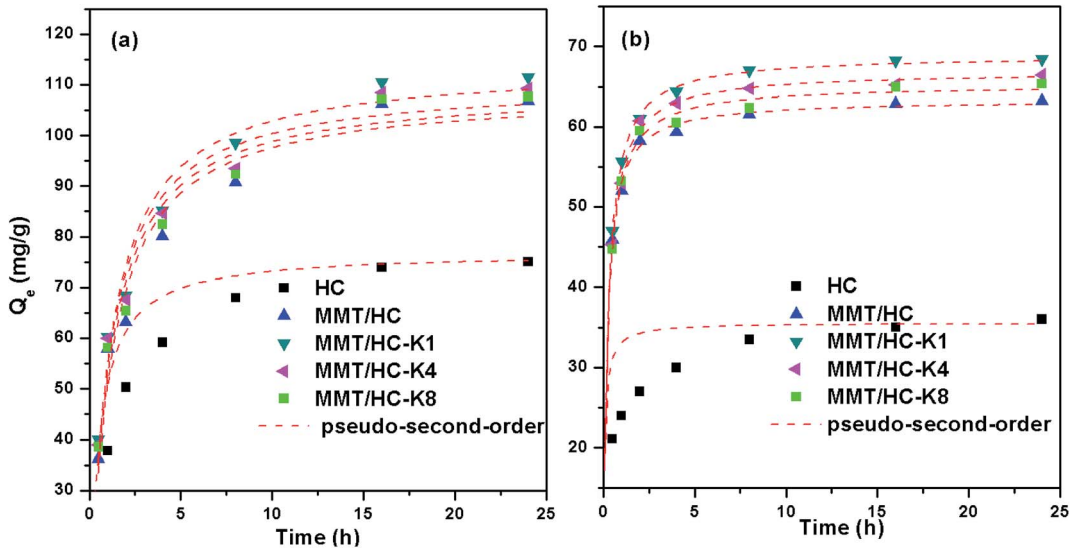

Fig. 7 Adsorption kinetics of E2 (a) and EE2 (b) adsorption on adsorbents.

that of the pseudo-first-order model and the Q_e values obtained by pseudo-second-order model were in agreement with the experimental adsorption data. These suggested that step could be dominated by chemical adsorption and physical adsorption as auxiliary. Such behaviors of adsorbent for removal estrogen were reported by various studies.[6,16,47]

3.2.2 Adsorption isotherm. Considering the best performance in estrogens adsorption, MMT/HC-K1 was selected as the representative of MMT/HCs. The adsorption data were fitted by Freundlich and Langmuir models which were the most extensively adopted adsorption isotherm models in aqueous solutions. Two models are given as following:

$$Q_e = K_F C_e^n \quad (3)$$

$$Q_e = \frac{K_L Q_m C_e}{1 + K_L C_e} \quad (4)$$

where Q_e (mg g^{-1}) is the amount of adsorbed E2 or EE2 in the solution at equilibrium, C_e (mg L^{-1}) is the adsorbed concentration reaching equilibrium, Q_m (mg g^{-1}) is maximum adsorption capacity of adsorbent and K_L (L g^{-1}) is the Langmuir constant.[48] K_F is the Freundlich coefficient and n is an indicator of adsorption intensity ((mg g^{-1}) (mg L^{-1})$^{-1/n}$).

The fitting results of Langmuir and Freundlich isotherm models are shown in Fig. 8. The isotherm parameters and their 95% confidence intervals are summarized in Table 4. The results showed that the maximum adsorption capacity of MMT/HC-K1 for E2 (Q_m = 138 mg g^{-1}) was higher than that of EE2 (Q_m = 69 mg g^{-1}), because E2 could have a stronger affinity on MMT/HC-K1 surface in aqueous. Meanwhile, the Q_m values of Langmuir model were corresponded well to the experimental data. The correlation coefficient (R^2) of Langmuir model was higher than that of Freundlich model, which suggested that the adsorption of estrogens was better fitted by Langmuir model. These could be due to the distribution of monolayer adsorption sites on the surface of MMT/HC-K1. Moreover, Table 5 presents the adsorption condition and maximum adsorption capacity for adsorption of E2 or EE2 on various adsorbent materials. Compared to MMT/HC-K1, these adsorbents possessed lower adsorption capacity and higher cost relatively, such as CNTs (multi-walled carbon nanotubes)[49] and GAC (granular activated carbon).[16]

Table 3 Adsorption kinetics parameters for the adsorption of E2 and EE2 on adsorbents

		Parameters	HC	MMT/HC	MMT/HC-K1	MMT/HC-K4	MMT/HC-K8
E2	Pseudo-first-order	Q_e (mg g^{-1})	74.4	98.1	103.3	100.4	99.12
		k_1 (1/h)	1.40	0.67	0.70	0.73	0.70
		R^2	0.923	0.836	0.856	0.849	0.843
	Pseudo-second-order	Q_e (mg g^{-1})	76.88	108.6	113.8	110.6	109.35
		k_2 (g mg^{-1} h^{-1})	0.026	0.0082	0.0083	0.0088	1.06
		R^2	0.991	0.952	0.967	0.962	0.959
EE2	Pseudo-first-order	Q_e (mg g^{-1})	32.86	60.79	65.77	63.93	62.43
		k_1 (1/h)	9.09	2.51	2.25	2.18	2.29
		R^2	0.66	0.814	0.842	0.877	0.864
	Pseudo-second-order	Q_e (mg g^{-1})	35.54	63.3	68.8	66.8	65.23
		k_2 (g mg^{-1} h^{-1})	0.29	4.37	2.21	1.87	0.23
		R^2	0.922	0.987	0.997	0.992	0.983

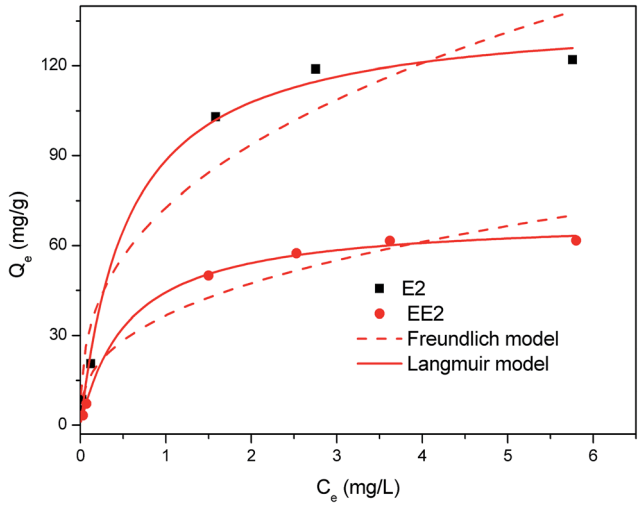

Fig. 8 Adsorption isotherms of E2 and EE2 adsorption over MMT/HC-K1.

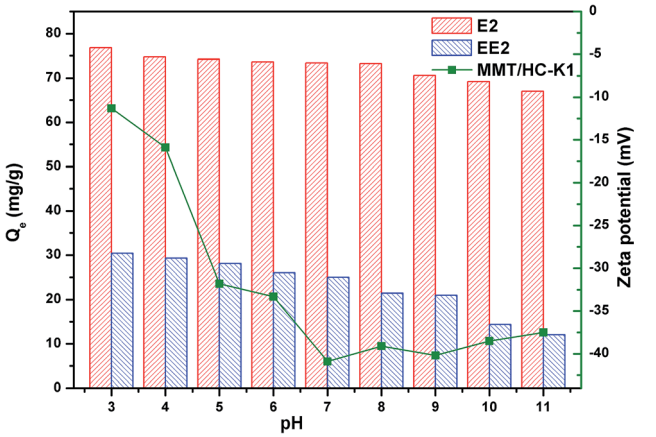

Fig. 9 Effect of solution pH on adsorption of E2 and EE2 on MMT/HC-K1 and its zeta potential at different pH.

Table 4 Adsorption isotherm parameters for the adsorption of E2 and EE2 over MMT/HC-K1

	Freundlich model			Langmuir model		
	K_f	$1/n$	R^2	Q_m (mg g^{-1})	K_L (L mg^{-1})	R^2
E2	73 ± 25	0.38 ± 0.23	0.922	138 ± 16	1.77 ± 1.03	0.994
EE2	37 ± 13	0.37 ± 0.25	0.915	69 ± 4	1.77 ± 0.60	0.998

3.2.3 Effect of initial pH. The pH is an important factor affecting adsorption process. The effect of initial pH on the zeta potentials of MMT/HC-K1 and estrogens removal ability were investigated. As shown in Fig. 9, the adsorption capacity of E2 maintained the relative maximum over a wide pH range (2–8). Nevertheless, the impact of pH had been altered, where the value of Q_e reduced to 67 mg g^{-1} at the basic solutions. As for EE2, it followed the same trend as E2. It also can be seen from Fig. 9 that the zeta potentials of MMT/HC-K1 held negative and electronegativity was decreased with the increase of pH values.

Considering the pK_a of E2 (~10.4)[50] and EE2 (~10.5),[2] most of E2 and EE2 would be in the protonated form with positive charge under the investigated conditions. At acidic condition, there was the H-binding interaction between hydroxyl group of E2 or EE2 and the functional groups on MMT/HC-K1 surface in adsorption process.[2] However, the relatively stable Q_e values of estrogens can be associated to stable H-bonding at those pH values. Similar results were reported by Seo *et al.* for adsorption of saccharin onto metal–organic framework.[51] The uptake was also depended upon ionization, which potentially promoted adsorption if the ionized molecules interacted more strongly with co-ordinated water molecules within the interlayer spaces of the mineral.[52] Moreover, the favorable interaction that electrostatic attraction between E2 or EE2 cation and the negative surface of MMT/HC-K1 could promote E2 or EE2 adsorption. At pH value above 8.0, the shifted trend of E2 and EE2 was relied on deprotonate to break the H-binding. When at basic solution, more OH^- ions could attract the proton on phenolic hydroxyl,[1] as well as compete with adsorption sites on MMT/HC-K1 surface. Moreover, it could be emerged that electrostatic repulsion between E2 or EE2 anion and the negative surface of MMT/HC-K1 and it will hinder E2 or EE2 adsorption.

Table 5 List of data for the adsorption of E2 and EE2 on various materials

Estrogen	Adsorbents	Initial concentration (mg L^{-1})	Temperature (°C)	pH	Maximum adsorption capacity (mg g^{-1})	References
E2	Waste cattle bones	5.0 or 9.0	25	—	10.12	47
	CNTs[a]	0.5–2.5	25 ± 1	—	11.5	60
	CNTs[a]	2.0	25 ± 1	6.3 ± 0.2	36.27	49
	MMT/HC-K1	6	25	7	138	This study
EE2	GAC[b]	0.05	30 ± 1	7	7.47 × 10^{-3}	16
	Polyamides	0.3	25	—	24.8	61
	Polyamide 612	0.2	25	—	16.1	62
	CNTs[a]	2.0	25 ± 1	6.3 ± 0.2	36.5	49
	MMT/HC-K1	6	25	7	69	This study

[a] CNTs = multi-walled carbon nanotubes. [b] GAC = granular activated carbon.

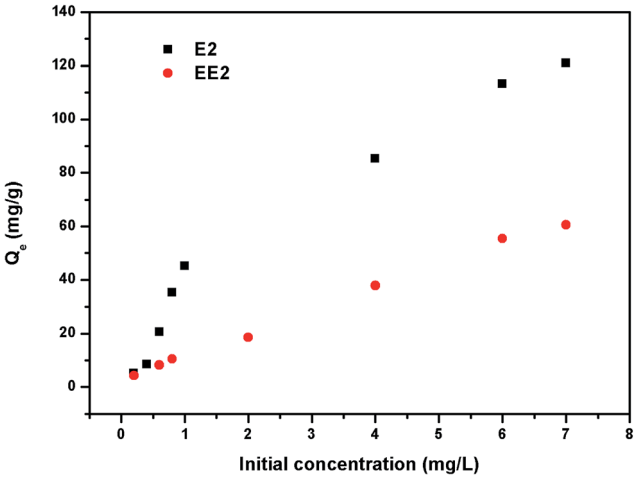

Fig. 10 Effect of initial concentrations on adsorption of E2 and EE2 on MMT/HC-K1.

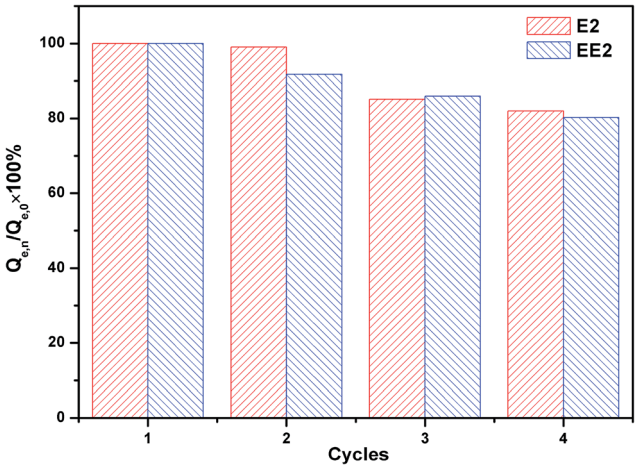

Fig. 12 Regeneration of MMT/HCs for the adsorption of E2 and EE2.

3.2.4 Effect of initial concentration. The adsorption amount of estrogens from water by MMT/HC-K1 is presented in Fig. 10. At relatively low estrogens initial concentrations, the adsorbent was more effective to remove E2 than that of EE2, since MMT/HC-K1 for adsorption of E2 might be admitted more binding sites to attach E2. The Q_e value of E2 and EE2 tend to stabilize with increasing initial estrogens concentration because of the saturation of adsorption sites and low availability of binding sites.[53]

3.3 Mechanism of estrogen adsorption

To understand the mechanism of E2 and EE2 adsorption by the MMT/HC-K1, the FTIR spectrum of materials before and after adsorption of estrogen were compared. As shown in Fig. 11, the vibration bands of MMT/HC-K1 showed apparently change before and after adsorption of E2 and EE2. On the one hand, the hydrogen bonded water molecule at 3436 cm^{-1} shifted to 3423 cm^{-1} and 3442 cm^{-1} after adsorption of E2 and EE2, respectively. The band of C=C at 1635 cm^{-1} shifted to 1639 and 1631 cm^{-1} after adsorption of E2 and EE2, respectively, which was confirmed the π–π interaction between estrogens and MMT/HC-K1. The band at 1388 cm^{-1} corresponding to C–O–H stretching shifted to 1382 and 1380 cm^{-1} after adsorption E2 and EE2, respectively, which implied the formation of hydrogen bonding between some oxygen-containing functional groups on MMT/HC-K1 surface and E2 or EE2. A similar phenomenon was reported by Chen *et al.*[31] On the other hand, four new bands at 3745, 2977, 2917 and 880 cm^{-1} were appeared in the spectra of MMT/HC-K1 after adsorption of E2, and one at 3733 cm^{-1} for that of EE2. Contrast to the FTIR spectra of pristine E2 or EE2, these new bands were originated from them. This could be ascribed to the intercalation of E2 or EE2 in the interlayer of montmorillonite through exchange reaction.[54]

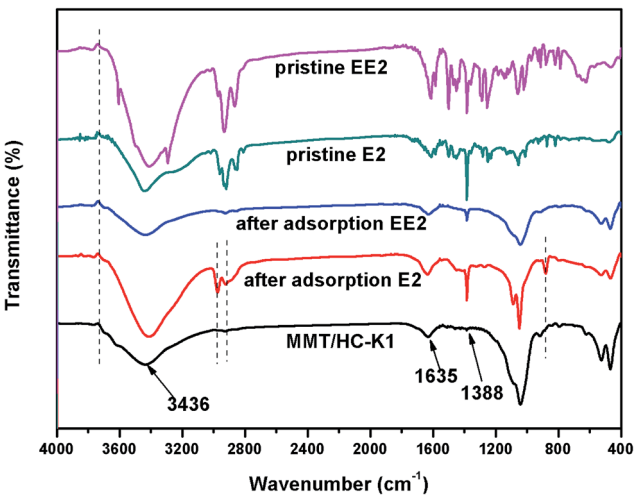

Fig. 11 FTIR spectra of E2, EE2 and MMT/HCs before and after adsorption of E2 or EE2.

Overall, the octanol–water distribution coefficient (K_{ow}) and solubility (S_W) implied the low volatility and hydrophobicity of estrogens (Table 1), which was an important factor to promote removal estrogens from water.[10,55,56] Moreover, the π–π interaction that a donor–acceptor system was formed between estrogen and MMT/HC-K1, and hydrogen bonding could account for estrogens adsorption. The electrostatic interaction between estrogens ion and the negative surface of MMT/HC-K1 could influence estrogens adsorption. In addition, the adsorption of estrogens did not depend on porosity and specific surface area to achieve a high adsorption capacity of most carbon adsorbents.[57]

3.4 Regeneration of MMT/HCs

The regeneration of adsorbent is a key criterion for practical applications in industry.[51] The regenerated MMT/HC-K1 for E2 and EE2 adsorptive removal were evaluated by conducting four cycle adsorption experiments. As shown in Fig. 12, the regenerated MMT/HC-K1 adsorbed E2 and EE2 effectively and the adsorption capacity was retained to 82% and 80.2% of its initial capacity after four cycles, respectively. The results

provided the preliminary evidences for the excellent reusability of MMT/HC-K1 for estrogens adsorption in aqueous environment.

4. Conclusions

In this work, the SEM, TEM and FTIR properties suggested that HC had been successfully synthesized with MMT. In addition, MMT/HCs had higher adsorption ability for E2 and EE2 than that of raw materials. MMT/HC-K1 exhibited the best adsorption efficiency, which had a remarkable maximum adsorption capacity for E2 (138 mg g^{-1}) and EE2 (69 mg g^{-1}). The adsorption capacity of estrogens maintained the relative maximum over a wide pH range (2–8). The composite increased the amount of oxygen-containing functional groups on MMT/HC-K1 surface. The favorable adsorption on MMT/HC-K1 could be explained by hydrophobicity, π–π bond, electrostatic interaction and H-bonding interaction. On the basis of regeneration performance, MMT/HCs could be reused for estrogens adsorption. As a result, MMT/HCs might be considered as a competitive and low-cost adsorbent for estrogens removal from aqueous environment.

Conflicts of interest

There are no conflicts to declare.

Acknowledgements

The present work was funded by the National Natural Science Foundation of China (Grants No. 51521006 and 51609268), the Hunan Provincial Innovation Foundation for Postgraduate (Grant No. CX2015B090 and CX2016B135), and the Key Project of Technological Innovation in the Field of Social Development of Hunan Province, China (Grant No. 2016SK2010 and 2016SK2001).

References

1 L. Jiang, Y. Liu, S. Liu, X. Hu, G. Zeng, X. Hu, S. Liu, S. Liu, B. Huang and M. Li, *Chem. Eng. J.*, 2017, **308**, 597–605.
2 Y. Feng, Z. Zhang, P. Gao, H. Su, Y. Yu and N. Ren, *J. Hazard. Mater.*, 2010, **175**, 970–976.
3 T. Fukuhara, S. Iwasaki, M. Kawashima, O. Shinohara and I. Abe, *Water Res.*, 2006, **40**, 241–248.
4 Z. Frontistis, C. Drosou, K. Tyrovola, D. Mantzavinos, D. Fatta-Kassinos, D. Venieri and N. P. Xekoukoulotakis, *Ind. Eng. Chem. Res.*, 2012, **51**, 16552–16563.
5 S. K. Khanal, B. Xie, M. L. Thompson, S. Sung, S. Ong and J. V. Leeuwen, *Environ. Sci. Technol.*, 2016, **38**, 6537–6546.
6 L. Jiang, Y. Liu, G. Zeng, F. Xiao, X. Hu, X. Hu, H. Wang, T. Li, L. Zhou and X. Tan, *Chem. Eng. J.*, 2016, **284**, 93–102.
7 D. G. J. Larsson, M. Adolfsson-Erici, J. Parkkonen, M. Pettersson, A. H. Berg, P. E. Olsson and L. Förlin, *Aquat. Toxicol.*, 1999, **45**, 91–97.
8 C. P. Silva, M. Otero and V. Esteves, *Environ. Pollut.*, 2012, **165**, 38–58.
9 M. Klavarioti, D. Mantzavinos and D. Kassinos, *Environ. Int.*, 2009, **35**, 402–417.
10 J. Li, L. Jiang, X. Liu and J. Lv, *Int. Biodeterior. Biodegrad.*, 2013, **76**, 3–7.
11 W. Ma, C. Nie, B. Chen, X. Cheng, X. Lun and F. Zeng, *J. Environ. Sci.*, 2015, **31**, 154–163.
12 E. McCallum, H. Hyung, T. Do, C. Huang and J. Kim, *J. Membr. Sci.*, 2008, **319**, 38–43.
13 W. Sun and K. Zhou, *Chem. Eng. J.*, 2014, **258**, 185–193.
14 J. Han, W. Qiu, Z. Cao, J. Hu and W. Gao, *Water Res.*, 2013, **47**, 2273–2284.
15 B. Jarosova, J. Filip, K. Hilscherova, J. Tucek, Z. Simek, J. P. Giesy, R. Zboril and L. Blaha, *J. Environ. Manage.*, 2015, **150**, 387–392.
16 K. Xu, W. F. Harper Jr and D. Zhao, *Water Res.*, 2008, **42**, 3146–3152.
17 L. Ai and L. Li, *Chem. Eng. J.*, 2013, **223**, 688–695.
18 X. F. Tan, Y. G. Liu, Y. L. Gu, Y. Xu, G. M. Zeng, X. J. Hu, S. B. Liu, X. Wang, S. M. Liu and J. Li, *Bioresour. Technol.*, 2016, **212**, 318–333.
19 A. Banerjee, R. Gokhale, S. Bhatnagar, J. Jog, M. Bhardwaj, B. Lefez, B. Hannoyer and S. Ogale, *J. Mater. Chem.*, 2012, **22**, 19694.
20 H. Wu, H. Xie, G. He, Y. Guan and Y. Zhang, *Appl. Clay Sci.*, 2016, **119**, 161–169.
21 T. M. Berhane, J. Levy, M. P. S. Krekeler and N. D. Danielson, *Appl. Clay Sci.*, 2016, **132–133**, 518–527.
22 B. N. Bhadra and S. H. Jhung, *ACS Appl. Mater. Interfaces*, 2016, **8**, 6770–6777.
23 Ö. Açışlı, S. Karaca and A. Gürses, *Appl. Clay Sci.*, 2017, **142**, 90–99.
24 A. Gürses, Ç. Doğar, M. Yalçın, M. Açıkyıldız, R. Bayrak and S. Karaca, *J. Hazard. Mater.*, 2006, **131**, 217–228.
25 Y. Yao, B. Gao, J. Fang, M. Zhang, H. Chen, Y. Zhou, A. E. Creamer, Y. Sun and L. Yang, *Chem. Eng. J.*, 2014, **242**, 136–143.
26 X. Tan, Y. Liu, G. Zeng, X. Wang, X. Hu, Y. Gu and Z. Yang, *Chem*, 2015, **125**, 70–85.
27 Y. Li, Z. Wang, X. Xie, J. Zhu, R. Li and T. Qin, *Colloids Surf., A*, 2017, **514**, 126–136.
28 Z. Liu and F.-S. Zhang, *J. Hazard. Mater.*, 2009, **167**, 933–939.
29 K. J. Kim, H. J. Kim, H. G. Park, C. H. Hwang, C. Sung, K. S. Jang, S. H. Park, B. G. Kim, Y. K. Lee, Y. H. Yang, J. H. Jeong and Y. G. Kim, *Sci. Rep.*, 2016, **6**, 24489.
30 Z. Zhang, Y. Feng, Y. Liu, Q. Sun, P. Gao and N. Ren, *J. Hazard. Mater.*, 2010, **181**, 1127–1133.
31 Q. Chen, R. Zhu, Y. Zhu, J. Liu, L. Zhu, L. Ma and M. Chen, *Appl. Clay Sci.*, 2016, **132–133**, 412–418.
32 M. Ejderkorucu, A. Gürses and S. Karaca, *Appl. Surf. Sci.*, 2016, **378**, 1–7.
33 D. Pottmaier, M. Costa, T. Farrow, A. A. M. Oliveira, O. Alarcon and C. Snape, *Energy Fuels*, 2013, **27**, 7115–7125.
34 T. Li, J. Shen, S. Huang, N. Li and M. Ye, *Appl. Clay Sci.*, 2014, **93–94**, 48–55.
35 Y. Zhu, H. R. Wang, X. X. Yang, W. Z. Cao, L. U. An-Huai, L. I. Yan, Q. H. Wang, X. L. Zhang and C. Q. Wang, *Acta Petrol. Mineral.*, 2011, **30**, 1053–1058.

36 P. Yuan, F. Annabi-Bergaya, Q. Tao, M. Fan, Z. Liu, J. Zhu, H. He and T. Chen, *J. Colloid Interface Sci.*, 2008, **324**, 142–149.
37 J. H. de Boer, B. C. Lippens, B. G. Linsen, J. C. P. Broekhoff, A. van den Heuvel and T. J. Osinga, *J. Colloid Interface Sci.*, 1966, **21**, 405–414.
38 S. Yang, M. Gao, Z. Luo and Q. Yang, *Chem. Eng. J.*, 2015, **268**, 125–134.
39 L. Wang and A. Wang, *Chem. Eng. J.*, 2008, **143**, 43–50.
40 J. Wang, Z. Chen and B. Chen, *Environ. Sci. Technol.*, 2014, **48**, 4817–4825.
41 M. Zhang, B. Gao, Y. Yao, Y. Xue and M. Inyang, *Chem. Eng. J.*, 2012, **210**, 26–32.
42 Y. Xu and B. Chen, *Bioresour. Technol.*, 2013, **146**, 485–493.
43 S. Kumar, V. A. Loganathan, R. B. Gupta and M. O. Barnett, *J. Environ. Manage.*, 2011, **92**, 2504–2512.
44 S. L. Chong, D. Wang, J. D. Hayes, B. W. Wilhite and A. Malik, *Anal. Chem.*, 1997, **69**, 3889–3898.
45 A. K. Kumar and S. V. Mohan, *Desalination*, 2011, **276**, 66–74.
46 J. Hu, S. Yang and X. Wang, *J. Chem. Technol. Biotechnol.*, 2012, **87**, 673–681.
47 S. Patel, J. Han and W. Gao, *J. Environ. Chem. Eng.*, 2015, **3**, 1562–1569.
48 A. C. Ijzer, E. Vriezekolk, E. Rolevink and K. Nijmeijer, *J. Chem. Technol. Biotechnol.*, 2015, **90**, 101–109.
49 W. Sun, C. Zhang, N. Xu and J. Ni, *Environ. Pollut.*, 2015, **205**, 111–120.
50 Y. Zhang and J. L. Zhou, *Water Res.*, 2005, **39**, 3991–4003.
51 P. W. Seo, N. A. Khan, Z. Hasan and S. H. Jhung, *ACS Appl. Mater. Interfaces*, 2016, **8**, 29799–29807.
52 A. Shareef, M. J. Angove, J. D. Wells and B. B. Johnson, *J. Colloid Interface Sci.*, 2006, **297**, 62–69.
53 M. Ahmad, S. S. Lee, X. Dou, D. Mohan, J.-K. Sung, J. E. Yang and Y. S. Ok, *Bioresour. Technol.*, 2012, **118**, 536–544.
54 Q. Wu, Z. Li, H. Hong, R. Li and W. T. Jiang, *Water Res.*, 2013, **47**, 259–268.
55 W. Ma, C. Nie, B. Chen, X. Cheng, X. Lun and F. Zeng, *J. Environ. Sci.*, 2015, **31**, 154–163.
56 A. Shareef, M. J. Angove, J. D. Wells and B. B. Johnson, *J. Colloid Interface Sci.*, 2006, **297**, 62–69.
57 J. Han, W. Qiu, S. Meng and W. Gao, *Water Res.*, 2012, **46**, 5715.
58 C. P. Silva, M. Otero and V. Esteves, *Environ. Pollut.*, 2012, **165**, 38–58.
59 Y. Feng, Z. Zhang, P. Gao, H. Su, Y. Yu and N. Ren, *J. Hazard. Mater.*, 2010, **175**, 970–976.
60 F. Lian, B. Sun, Z. Song, L. Zhu, X. Qi and B. Xing, *Chem. Eng. J.*, 2014, **248**, 128–134.
61 J. Han, W. Qiu, S. Meng and W. Gao, *Water Res.*, 2012, **46**, 5715–5724.
62 J. Han, W. Qiu, Z. Cao, J. Hu and W. Gao, *Water Res.*, 2013, **47**, 2273–2284.